Chapter 5

Beam monitoring: analysis and results

5.1 Overview

With the new high-intensity accelerator beam facilities becoming more and more powerful, while attempting measurements at increasingly high precision, real time beam monitoring is becoming essential, both to protect equipment, and to precisely measure beam properties. The simulations and analysis performed for this thesis aim to evaluate the beam monitoring capabilities of SAND for the DUNE muon neutrino beam.
Many of the beam characteristics can be used for beam monitoring. For this study we have considered the reconstructed momenta of muons produced in ν_μ CC interactions in SAND's front electro-magnetic calorimeter modules. The shape of the reconstructed energy spectrum of the muons produced in CC interactions, depends on the original ν_μ energy spectrum. Any anomalies in the beam production would thus in principle cause variations in both spectra. In particular we considered the anomalies generated when the second neutrino beam horn experienced a transverse displacement of +0.05mm in the Y coordinate
The nominal and modified interactions samples were simulated using the GENIE neutrino MonteCarlo generator to have vertex in one of the eight frontal barrel calorimeter modules. The particles produced in the interactions were then propagated with edep-sim, the ECAL and STT signals were digitized and the clusters and tracks reconstructed. Note that in order to shorten the simulation times the digitization and reconstruction steps were performed only on the primary particles of the interactions.
No particle identification has been implemented for SAND's simulation chain

at the time of writing. The muon tracks where thus selected post reconstruction from the MonteCarlo truth PID informations. In order to select only the muons produced in CC interactions in the inner layers of the calorimeter, a selection on the energy deposition on the most outer layer of the ECAL was implemented. This energy deposition threshold, together with a selection on the x position of the neutrino vertexes defined our fiducial cut.
Only the correctly reconstructed momenta were considered. Additionally the χ^2 values for the linear and circular fits were used to identify a reconstruction quality selection.
We studied the sensitivity to the beam modification by applying two-sample homogeneity tests on the reconstructed muon momentum distributions on samples roughly corresponding to the amount of CC interactions expected in the front calorimeters of SAND in a week, as suggested by the ND collaboration for beam monitoring measures. Given the number of interactions per second expected in a calorimeter module ϵ, and the number of target modules $n_{mod} = 10$ this corresponds to:

$$N_{week} = \epsilon \times n_{mod} \times 3600s \times 7gg. \simeq 1.7 \times 10^6 \tag{5.1}$$

5.2 Preliminary measurements

A series of preliminary measurements were needed before the application of the beam monitoring tests. Firstly we needed to extrapolate the calibration coefficient between the energy loss of a muon in a calorimeter module cell and the total number of photo-electrons produced. This was essential to be able to set the p.e. threshold used for the outer layer cut.
An evaluation of the reconstruction algorithm efficiency with respect to energy was also needed, together with a study on the efficiency of the front layer energy deposition cut and reconstruction selection.

5.2.1 Muon energy loss calibration

In order to measure the calibration constant between the muon energy loss and the photo-electron production in the calorimeter cells, we simulated a set of 1000 muons with an initial energy of 10 GeV, hitting a calorimeter barrel module at the centre of one of its front cells. The muons were generated using a simple GEANT4 particle gun via $edep - sim$, while the geometry containing the single calorimeter module was produced using *gegede* exactly in the same way as for the entire ECAL. A graphical representation of one of these events is shown in Figure 5.1. Both the particle gun and the module

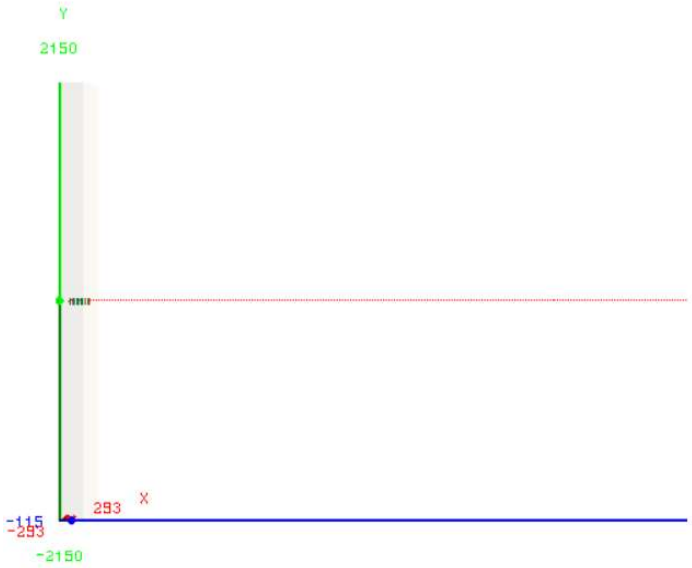

Figure 5.1: A 10 GeV muon hitting a calorimeter module simulated using the edep-sim GEANT4 particle gun option and drawn using edep-disp. The red line indicates the muon track, with the hits inside the calorimeter highlighted in green. The coordinates are in millimeters.

were placed in vacuum.
The hits and relative energy losses were then assigned to the calorimeter cells during digitization producing two ADC values for each cell. The distribution of the sum of the two ADC values, which in our simple digitization algorithm corresponds with the total production of photo-electrons, is shown in Figure 5.2. Performing a Landau fit on the histogram we find that the most probable value is:

$$N_{p.e.}^{cell} = (97.39 \pm 0.34) \tag{5.2}$$

We can approximate the energy loss of the muon with the one experienced by a minimum ionizing particle (MIP) traversing 40 slabs of lead for a total of $\Delta x_{Pb} = 1.6$ cm and 40 slabs of plastic scintillator for a total thickness of $\Delta x_{Sc} = 2.8$ cm:

$$\Delta E_{cell} \simeq \left(\frac{dE}{dx}\right)^{MIP} \rho_{Pb} \Delta x_{Pb} + \left(\frac{dE}{dx}\right)^{MIP} \rho_{Sc} \Delta x_{Sc} \simeq 42.22 \text{ MeV} \tag{5.3}$$

where $(dE/dx)^{MIP} \sim 2\text{MeV}/(\text{g/cm}^2)$ is the average energy loss of a MIP and $\rho_{Pb} = 11.34$ g/cm^3 and $\rho_{Sc} = 1.06$ g/cm^3 are the densities of lead and the scintillating material respectively.

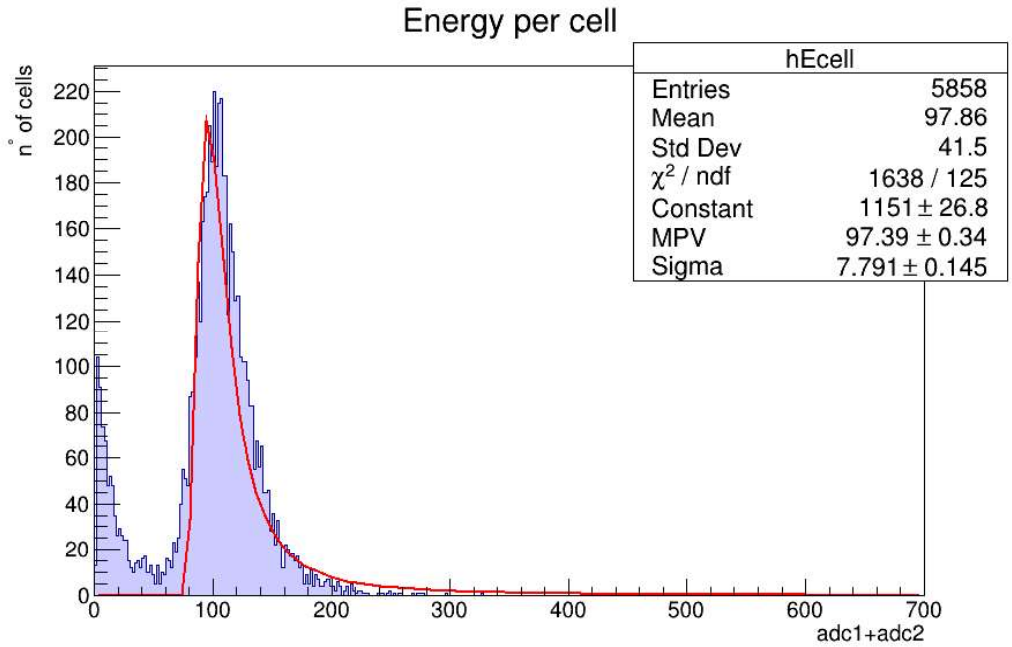

Figure 5.2: Distribution of total number of photo-electrons produced at the passage of a 10 GeV muon in a ECAL cell. The histogram has been produced from a set of 1000 muons simulated hitting a calorimeter module. These were generated using the GEANT4 particle gun mode implemented in edep-sim. The red line indicates a Landau fit, the results of which are summarized in the box in the upper right corner of the histogram canvas.

The average number of photo-electrons produced per cell per MeV is given by the calibration coefficient:

$$c = \frac{N_{p.e.}^{cell}}{\Delta E_{cell}} \simeq 2.31 \text{ [p.e./Mev]} \tag{5.4}$$

This is roughly in agreement with previous calibrations performed by the KLOE collaboration using cosmic ray muons, which measured an average number of p.e. per ADC per MeV of about 1 p.e./MeV.

5.2.2 Fiducial cut

Selecting from the total one week nominal sample of 1.7×10^6 events, only the CC interactions, we are left with 1276447 events. All the muons in this sample are the product of CC interactions in the front calorimeter modules. In a realistic physical scenario, the sample would include also a

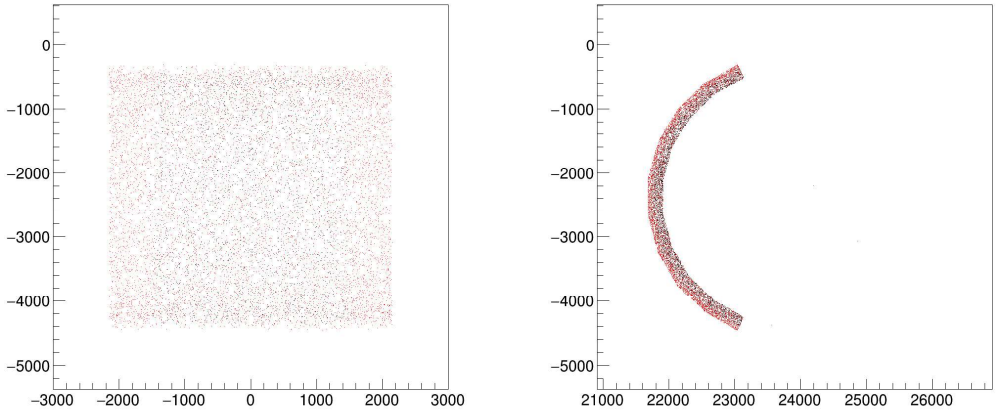

(a) (b)

Figure 5.3: Spatial distribution in ND hall global coordinates of the neutrino interaction vertexes of the events that survive the outer layer cut (black) and the events having their vertex in the outer layer from the Montecarlo truth (red). The two panels show the projection (a) on the xy plane and (b) on the yz plane.

certain amount of muons that are the product of ν_μ CC from outside the detector either from the neutrino beam or from cosmic rays.
In order to eliminate these external events from our sample we introduce an energy deposition threshold on the outer layer of $\Delta E_{th} = 15$ MeV. Using the conversion coefficient found in Section 5.2.1 we then find the threshold in number of total photo-electrons produced:

$$N_{p.e.}^{th} = c \times \Delta E_{th} \simeq 35 \text{ p.e.} \tag{5.5}$$

Any event having photo-electron production on the outer layer ≥ 35 p.e. is eliminated.

In order to eliminate those events that are likely going to produce muons that won't fully traverse the STT, which we expect to have poor momentum reconstruction, we also define a spatial cut on the x position of the interaction vertex:

$$|x_V| \leq 1.5 \text{ m} \tag{5.6}$$

In order to estimate the vertex position we use the space information from those front calorimeter modules' cells in which there has been an energy deposition. Specifically we evaluate x_V as a weighted average on the ADC

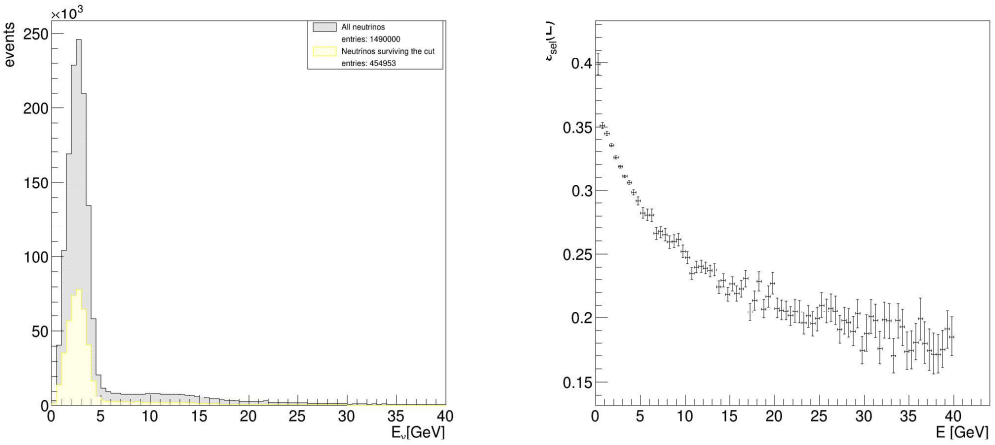

(a) (b)

Figure 5.4: (a) Energy (Montecarlo truth) distribution of neutrinos from the CC nominal sample (grey); Energy (Montecarlo truth) distribution of neutrinos surviving the fiducial cut (yellow) (b) Selection efficiency as a function of neutrino energy from the Montecarlo truth.

deposits E_i^{cell}:

$$x_V = \frac{\sum_{i=1}^{N_{cell}} x_i^{cell} E_i^{cell}}{E_{tot}^{cell}} \tag{5.7}$$

N_{cell} is the number of hit cells, x_i^{cell} is the estimated position of the particle transit within the cell and E_{tot}^{cell} is the total ADC p.e. production in the front calorimeter modules.
We define the combination of the outer layer energy deposition and the vertex selection as our fiducial cut.
In Figure 5.3 we show the spatial distribution of the interaction vertexes of the events surviving the fiducial cut (black), together with the full CC sample events (red). In Figure 5.4 (a) we show the distribution in neutrino energy from the Montecarlo truth of the events before and after the cut.
We can define now the cut efficiency ε_{cut} as the ratio between the events surviving the selection N_{fid} and the total number of CC events N:

$$\varepsilon_{cut} = \frac{N_{fid}}{N} = 0.305 \tag{5.8}$$

The selection efficiency distribution with respects to the neutrino energy is shown in Figure 5.4 (b). Note that ε_{cut} gets worse at higher energy. This is might be due to nuclei fragmentation in DIS ν_μ which produce a large quantity of scattered nucleons that can deposit energy in the calorimeter.

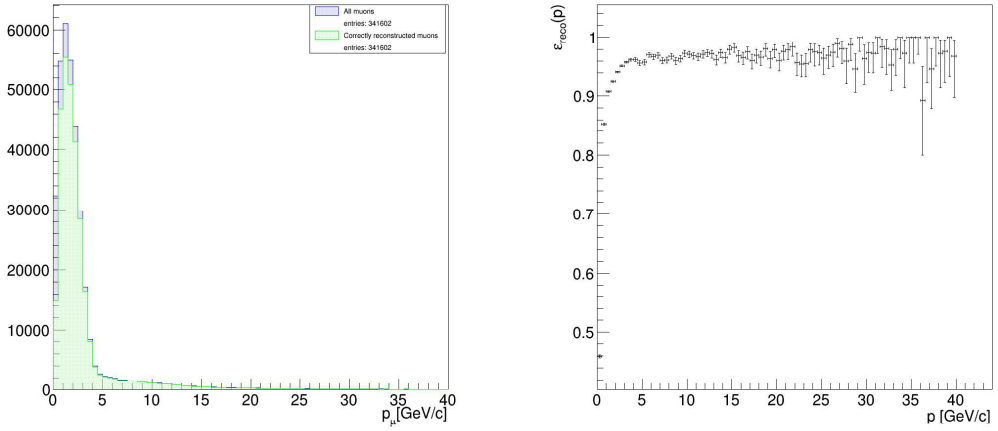

(a) (b)

Figure 5.5: (a) Distributions of the true momenta of the muons from the fiducial sample (blue) and only the ones correctly reconstructed (green) (b) Reconstruction algorithm efficiency as a function of the muon momentum from the Montecarlo truth.

5.2.3 Muon track reconstruction efficiency

The STT track reconstruction algorithm described in Section 4.5 can sometimes fail. If either one of the two fits fail, the reconstruction is considered unsuccessful and the event is flagged and discarded for the final momentum reconstruction.
The circular fit is considered not successful if the track has less than three hits on horizontal straw tubes or if problems occurred in assigning the coordinate values to any of the straw hits or in any of the passages of the fit algorithm (like for example having a 0 value as a denominator). The linear fit always fails if the circular fit is unsuccessful, since it necessitates the (y_C, z_C) and R estimates in order to calculate the ρ coordinates. The other failure conditions are analogous to the circular fit ones, with additional problems occurring when extrapolating the y coordinate from the x and z values obtained from the vertical straws.
The total reconstruction efficiency is given by the ratio between the number of correctly reconstructed muons $N_{reco} = 299988$ and the total number of muons in the fiducial sample $N_{fid} = 341602$:

$$\varepsilon_{reco} = \frac{N_{reco}}{N_{fid}} = 0.878 \tag{5.9}$$

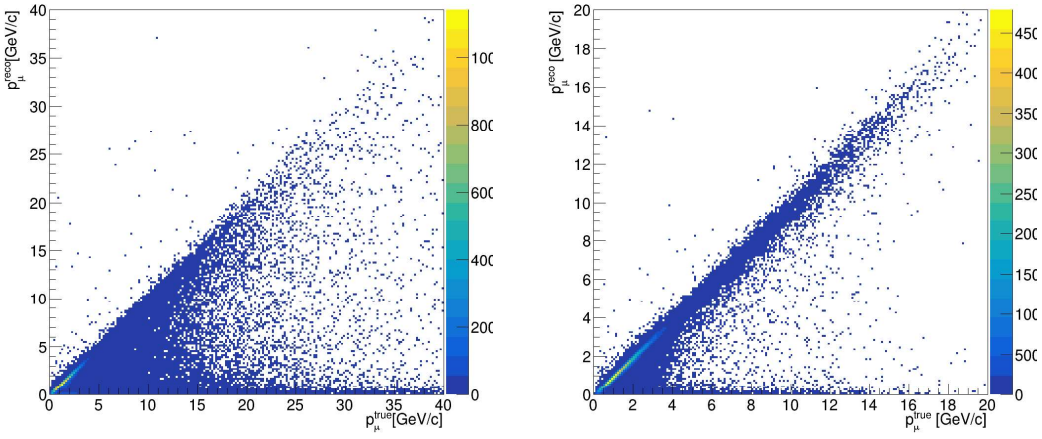

(a) (b)

Figure 5.6: Reconstructed momenta as a function of the real ones, before (a) and after (b) the quality cut is applied

In Figure 5.5 (a) we show the distribution of the muon real momenta from the two samples and in Figure 5.5 (b) we show ε_{reco} as a function of the muon momentum.

5.2.4 Quality selection

By plotting the reconstructed muon momentum of those events for which the track fits were considered successful (Figure 5.6 (a)), we see that in a considerable amount of cases, especially at low energies, p_μ is underestimated. We might then want to apply a cut on the χ^2 values of the linear and/or circular fits in order enhance the average quality of the reconstruction in our sample. We try to gauge what such a cut might be by plotting the linear χ^2 as a function of longitudinal momentum, and the circular χ^2 as a function of transverse momentum (Figure 5.7 (a) and (b) respectively). From these plots and proceeding by trial and error we found the selection:

$$\chi^2_{lin} < 10^5 \tag{5.10}$$

In Figure 5.6 (b) we show the reconstructed momenta as a function of the real momenta after the quality cut is applied. The efficiency of this selection is given by the ratio between the number of events having sufficiently small χ^2 values N_{qual} and the total amount of reconstructed muons N_{reco}:

$$\varepsilon_{qual} = \frac{N_{qual}}{N_{reco}} = \frac{223578}{290906} = 0.769 \tag{5.11}$$

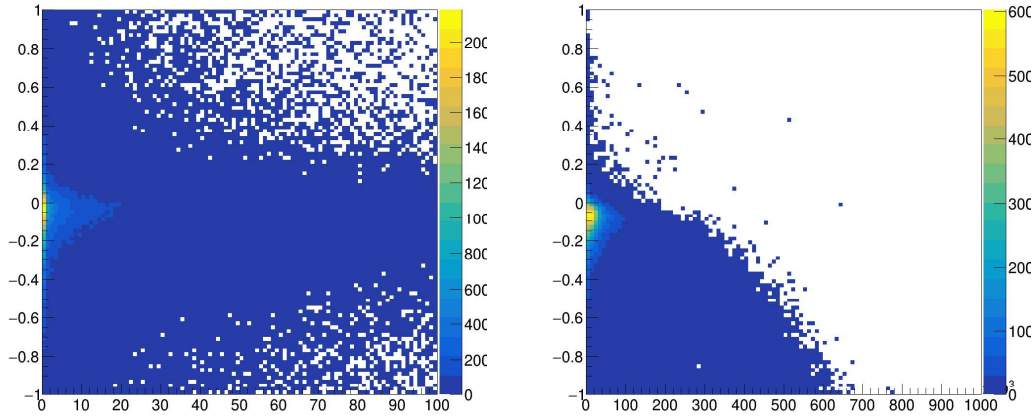

(a) (b)

Figure 5.7: (a)Linear χ^2 as a function of longitudinal momentum; (b) Circular χ^2 as a function of transverse momentum. The fiducial cut and reconstruction successfulness cuts have both been applied to the samples.

While the statistical reduction of the sample is significant, the plots seem to indicate an improvement in the accuracy of the momentum evaluation.

5.3 Beam monitoring study results

To perform the beam monitoring measurements, we considered the muon neutrino flux produced by the neutrino beam in standard conditions and we confronted it with the one generated when the second horn had a transverse displacement of +0.05mm in the Y coordinate. The corresponding neutrino fluxes simulated by the Beam facilities group as a function of energy in units of $\nu_\mu/m^2/POT/\text{GeV}$ are shown in Figure 5.8.
Note that the ν_μ fluxes were also generated by the collaboration with modifications to many other critical parameters. These include: transverse displacement in both horns and the proton beam; modifications in the proton beam radius and angle on target; shifts in the values of the decay pipe radius, horn currents, target density and horn water layer thickness. The critical parameter for this study has been selected arbitrarily and is not of special interest over any of the others.

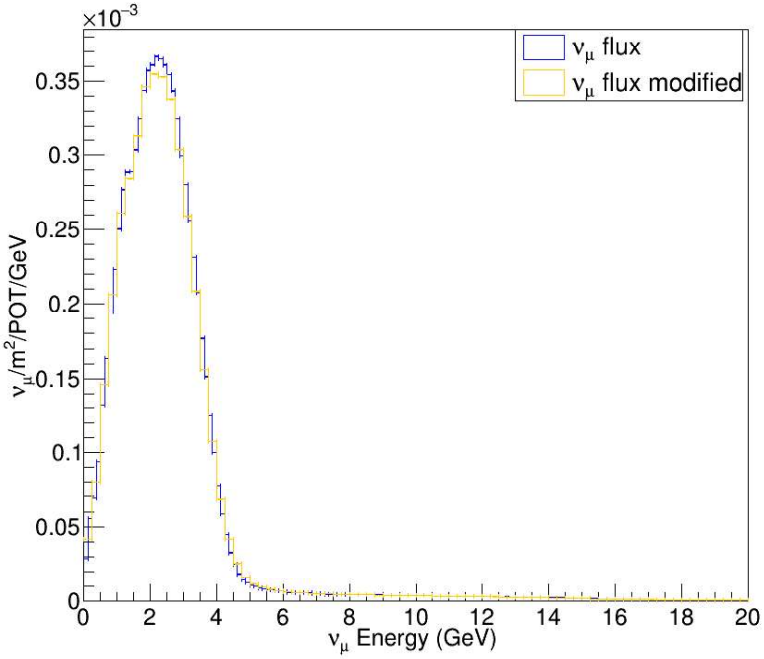

Figure 5.8: (Blue) Muon neutrino flux as a function of neutrino energy produced by the DUNE neutrino beam in standard conditions (Orange) Muon neutrino flux as a function of neutrino energy generated when the second horn had a transverse displacement of +0.05mm in the Y coordinate.

5.3.1 Two-sample statistical tests test

In order to spot an anomaly in the neutrino beam production, we would like to test if the modified muon energy spectrum is not consistent with the original one i.e. if the hypothesis that the two histograms are sampled from the same distributions is incorrect. We do not have a clearly defined null hypothesis for what the common distribution would be, so we can only compare the two histograms bin by bin with a so called two-sample statistical test. Of the many possible tests that exist we decided to use three: the χ^2 test, which is a valid two-sample test in the large sample approximation; the Kolmogorov-Smirnov test; the Anderson-Darling test. We implemented the first as a C++ algorithm, while for the second and third we used the ROOT functions KolmogorovTest and AndersonDarlingTest. Since the χ^2 test is the only one directly implemented by us, the p-values obtained with it will be treated as the reference.

Two-sample χ^2 test

Given two histograms with the same number of bins k and boundaries, the bin contents are the realisations of two random variables U and V. If we call u_i and v_i the realizations of the bin contents and μ_i and ν_i, the bin contents distributions have the shapes of Poisson functions. The sampling distributions of the two histograms are thus:

$$P(U = u) = \prod_{i=1}^{k} \frac{\mu_i^{u_i}}{u_i!} e^{-\mu_i} \tag{5.12}$$

$$P(V = v) = \prod_{i=1}^{k} \frac{\nu_i^{v_i}}{v_i!} e^{-\nu_i} \tag{5.13}$$

The hypothesis that the two histograms follow the same distribution is equivalent to saying that there are k constants p_i that are the probabilities of belonging to the ith bin for both histograms, so that:

$$\sum_{i=1}^{k} p_i \tag{5.14}$$

Given the total number of entries for each histogram $N_u = \sum u_i$ and $N_v = \sum v_i$, then the probability of observing u_i events in the ith bin of the first histogram and the probability of observing v_i events in the ith bin of the second histogram given by:

$$\frac{e^{-N_u p_i}(N_u p_i)^{u_i}}{u_i!} \tag{5.15}$$

$$\frac{e^{-N_v p_i}(N_v p_i)^{v_i}}{v_i!} \tag{5.16}$$

If the hypothesis of compatibility between the two histograms is correct the maximum likelihood estimator of p_i is:

$$\hat{p}_i = \frac{u_i + v_i}{N_u + N_v} \tag{5.17}$$

We can then construct the test statistic:

$$T = \sum_{i=1}^{k} \frac{(u_i - N_u \hat{p}_i)^2}{N_u \hat{p}_i} + \sum_{i=1}^{k} \frac{(v_i - N_v \hat{p}_i)^2}{N_v \hat{p}_i} = \frac{1}{N_u M_v} \sum_{i=1}^{k} \frac{(N_u u_i - N_v v_i)^2}{u_i + v_i} \tag{5.18}$$

T follows approximately a χ^2 distribution for $k-1$ degrees of freedom, as long as we are in a situation where the two samples are large enough that the bin contents are distributed normally. We can thus estimate from the χ^2 distribution, the p-value, which in this case is the probability of having two histograms that are as much or less in agreement than the ones we are testing, if they are sampled from the same distribution.

Kolmogorov-Smirnov test

The two-sample Kolmogorov-Smirnov test consists in measuring the maximum difference between the two cumulative distribution functions (CDFs) and compare with the null homogeneity hypothesis expectations.
We approximate the cumulative distribution functions as histograms:

$$u_{ci} = \sum_{j=1}^{i} u_j / N_u \tag{5.19}$$

$$v_{ci} = \sum_{j=1}^{i} v_j / N_v \tag{5.20}$$

The test statistic is then given by:

$$T_{KS} = \max_i |u_{ci} - v_{ci}| \tag{5.21}$$

The null hypothesis is rejected at significance level α if:

$$T_{KS} \geq c(\alpha) \sqrt{\frac{N_u + N_v}{N_u \cdot N_v}} \tag{5.22}$$

where $c(\alpha)$ is the inverse of the Kolmogorov distribution and in general can be calculated approximately as:

$$c(\alpha) = \sqrt{-\ln(\alpha/2) \cdot (1/2)} \tag{5.23}$$

Note that the Kolmogorov-Smirnoff test tends to emphasize differences near the peak of the distribution, where the largest fluctuations are expected for Poisson probabilities.

The Anderson-Darling test

The Anderson-Darling test is a modified version of the Kolmogorov-Smirnov test design to improve the sensitivity to the tails of the CDFs. The original statistical test, designed to test the compatibility of a data set

x having an empirical CDF $F_m(x)$, with a continuous distribution, having the CDF $F_0(x)$ under the null hypothesis is:

$$A_m^2 = m \int_{-\inf}^{\inf} \frac{[F_m(x) - F_0(x)]^2}{F_0(x)[1 - F_0(x)]} dF_0(x) \tag{5.24}$$

Scholz and Stephens adapted this statistic to the k-sample case, which in our simple two-sample situation reads:

$$T_{AD} = \frac{1}{N_u + N_v} \sum_{j=k_{min}}^{k_{max}-1} \frac{u_j + v_j}{\Sigma_j (N_u + N_v - \Sigma_j)} \times \left[((N_u + N_v)\Sigma_{uj} - N_u \Sigma_j)^2 / N_u + ((N_u + N_v)\Sigma_{vj} - N_v \Sigma_j)^2 / N_v \right] \tag{5.25}$$

where k_{min} is the first non-zero bin for both histograms, k_{max} is the number of bins until the last non-zero bin and:

$$\Sigma_{uj} = \sum_{i=1}^{j} u_i; \quad \Sigma_{uj} = \sum_{i=1}^{j} u_i; \tag{5.26}$$

$$\Sigma_j = \sum_{i=1}^{j} (u_i + v_i) = \Sigma_{uj} + \Sigma_{vj} \tag{5.27}$$

5.3.2 The control samples

As a first control of the methodology we decided to apply the χ^2 test to the reconstructed momenta from two samples simulated from the nominal neutrino beam. If the method is capable of distinguishing between the products of two different neutrino beam configuration, we expect to obtain a p-value for two control samples that follow the same distribution that is close to 1. We derive the two samples by applying the fiducial cut and momentum reconstruction control to the one week simulation and dividing it randomly into to groups (the correspondent momenta distributions are plotted in Figure). We thus obtain the and p-value:

$$p_{control} = 0.698 \ (\chi^2) \tag{5.28}$$

$$\sigma_{control} = 0.388 \ (\chi^2) \tag{5.29}$$

where the number of degrees of freedom is given by the number of bins in the histograms minus 1: $n.d.f. = 39$.
The correspondent p-values were obtained for the Kolmogorov-Smirnov (K.S.)

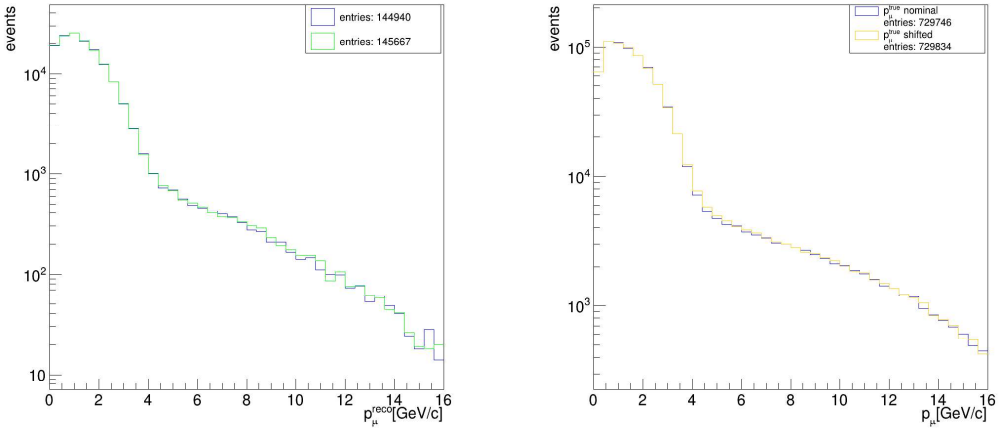

(a) (b)

Figure 5.9: (a)Reconstructed momenta distributions from two control half-statistics samples produced with the nominal neutrino beam. The fiducial cut and momentum reconstruction control are applied (b) Real momenta distributions from the nominal and shifted samples. A fiducial cut on the true vertexes is applied. Both histograms are in logarithmic scale.

and Anderson-Darling (A.D.) test using more finely binned histograms ($n_{bin} = 1000$), as suggested on the ROOT reference manual:

$$p^{KS}_{control} = 0.554; \qquad \sigma^{KS}_{control} = 0.591\ (K.S.) \tag{5.30}$$

$$p^{AD}_{control} = 0.561; \qquad \sigma^{AD}_{control} = 0.581\ (A.D.) \tag{5.31}$$

As a second control we decided to apply the test to the real momenta from the nominal and shifted samples. A fiducial cut was applied by selecting only the CC events whose vertexes were not on the outer layer of the calorimeter and for which $|x_V^{truth}| < 1.5$ m (the two distributions are plotted in Figure 5.9). This was done in order to gauge what the best possible p-value (i.e. the smallest and most decisive) might be:

$$p_{truth} = 3.56 \times 10^{-7}; \qquad \sigma_{truth} = 5.09\ (\chi^2) \tag{5.32}$$

$$p^{KS}_{truth} = 2.45 \times 10^{-4}; \qquad \sigma^{KS}_{truth} = 3.67\ (K.S.) \tag{5.33}$$

$$p^{AD}_{truth} = 6.80 \times 10^{-4}; \qquad \sigma^{AD}_{truth} = 3.40\ (A.D.) \tag{5.34}$$

No p-value obtained from the reconstructed momenta should be smaller than p_{truth}.

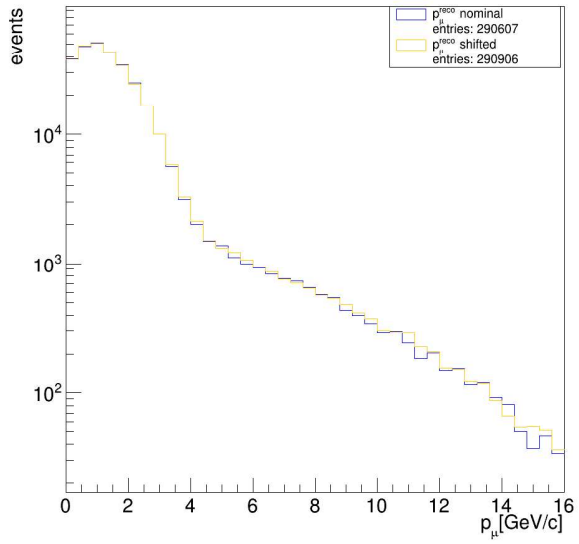

t!

Figure 5.10: True momenta distributions from the nominal and shifted samples.The fiducial and reconstruction selections are applied. Both histograms are in logarithmic scale.

5.3.3 Results

The first two samples considered for beam monitoring are the muon reconstructed momenta after the fiducial cut and the selection on the successfulness of the reconstruction are applied. The reconstructed momentum distributions of the muons produced with nominal and shifted neutrino fluxes are shown in Figure 5.10.
Applying the statistical tests on the reconstructed momenta samples we find:

$$p_{reco} = 3.68 \times 10^{-3}; \qquad \sigma_{truth} = 2.90(\chi^2) \tag{5.35}$$
$$p_{reco}^{KS} = 0.232; \qquad \sigma_{truth}^{KS} = 1.19(K.S.) \tag{5.36}$$
$$p_{reco}^{AD} = 0.130; \qquad \sigma_{truth}^{AD} = 1.52(A.D.) \tag{5.37}$$

We repeat the procedure by applying the quality cut described in Section 5.2.4 to both samples (reconstructed momentum distributions for the new samples are shown in Figure 5.11). The new p-values and significance levels from the reconstructed samples are:

$$p_{reco} = 1.45 \times 10^{-4}; \qquad \sigma_{reco} = 3.80(\chi^2) \tag{5.38}$$
$$p_{reco}^{KS} = 0.231; \qquad \sigma_{reco}^{KS} = 1.20(K.S.) \tag{5.39}$$
$$p_{reco}^{AD} = 0.100; \qquad \sigma_{reco}^{AD} = 1.64(A.D.) \tag{5.40}$$

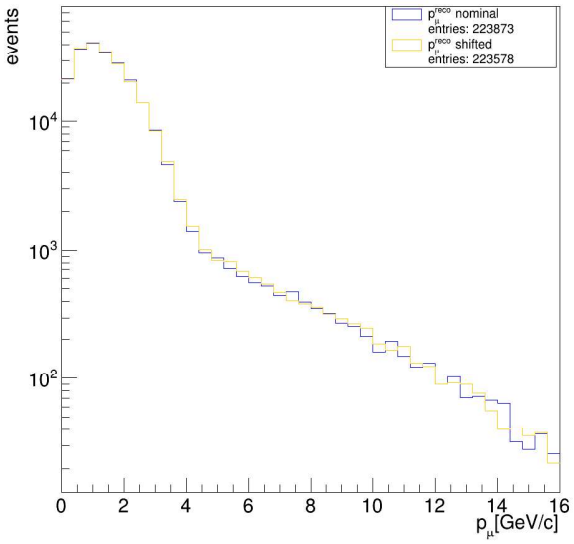

Figure 5.11: Reconstructed momenta distributions from the nominal and shifted samples. The fiducial, reconstruction and quality selections are applied. Both histograms are in logarithmic scale.

Evolution of p-value and sigma with the sample

In order to study how the p-value and significance level grew with the data, we applied the χ^2 to increasingly larger samples. We show the results for quality cut reconstructed momenta samples and fiducial true momenta samples in Figure 5.12.
As we should expect as the samples become larger the χ^2 and number of σ's grow, while the p-value decreases. We also notice that the growth in confidence level i.e. number of σ's seems to slow down after we reach a sample of $\sim 10^6$ CC events.

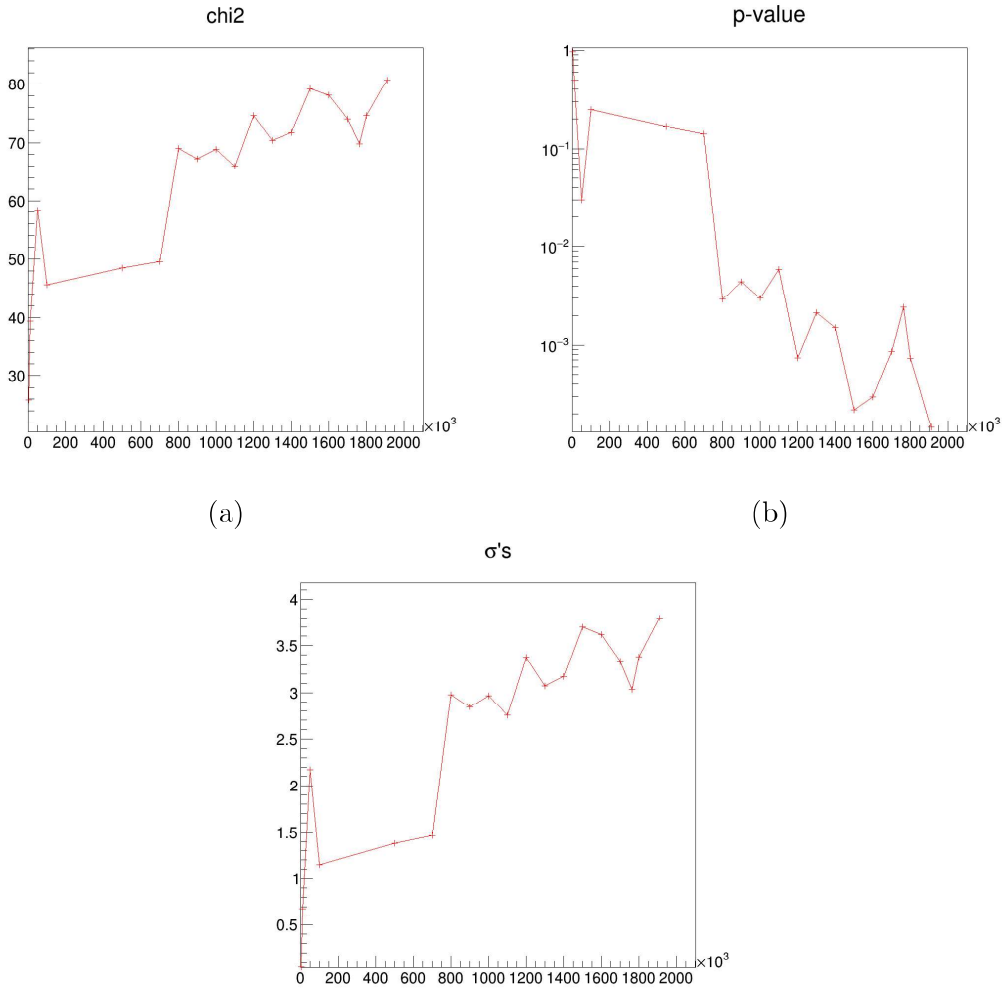

(a) (b)

(c)

Figure 5.12: Evolution of the values of (a) χ^2, (b) p-value, (c) number of sigmas for increasingly larger samples where all the cuts were applied. The graphs are in logarithmic scale